Water in Earth's Lower Mantle

Motohiko Murakami,[1]* Kei Hirose,[1] Hisayoshi Yurimoto,[1] Satoru Nakashima,[2] Naoto Takafuji[1]

Secondary ion mass spectrometry measurements show that Earth's representative lower mantle minerals synthesized in a natural peridotitic composition can dissolve considerable amounts of hydrogen. Both $MgSiO_3$-rich perovskite and magnesiowüstite contain about 0.2 weight percent (wt%) H_2O, and $CaSiO_3$-rich perovskite contains about 0.4 wt% H_2O. The OH absorption bands in Mg-perovskite and magnesiowüstite were also confirmed with the use of infrared microspectroscopic measurements. Earth's lower mantle may store about five times more H_2O than the oceans.

The mass of the oceans is only 0.02% of that of Earth. If Earth was formed by the mixture of C1 chondrite and enstatite chondrite (*1*), it initially contained about 2 wt% H_2O. Most of the H_2O (or reduced H) may have been lost from Earth since then, or it may still be stored in Earth's deep interior. If H_2O is present in the interior, it will influence the physical and chemical properties of the silicate mantle such as its viscosity (*2*), melting temperature (*3*, *4*), rate of ionic diffusion, and grain growth. Previous experiments on the maximum solubility of H_2O or hydrogen in mantle minerals and molten iron at high pressures showed that wadsleyite and ringwoodite can include 2 to 3 wt% of H_2O in the transition zone (*5*–*7*) and that molten iron can dissolve ~4% hydrogen (*8*). However, the possible sites for H_2O in lower mantle minerals have been controversial. The dense hydrous magnesium silicate (DHMS) phase of phase D contains more than 10 wt% H_2O in the lower mantle, but it is stable only in cold slabs at depths shallower than 1200 km (*9*). The lower mantle is believed to consist predominantly of Mg-perovskite with some magnesiowüstite and Ca-perovskite (*10*, *11*). Elucidating the water contents in these minerals will lead to an understanding of the most promising storage site of H_2O in the lower mantle. It was suggested that Mg-perovskite was a potential candidate for water storage in the deep mantle (*12*–*14*). Previous infrared spectroscopic measurements showed that the solubility of water in pure $MgSiO_3$-perovskite is quite limited or undetectable (*15*, *16*). However, it is well understood that the water in nominally anhydrous minerals such as olivine, pyroxene, garnet, and their high-pressure polymorphs is likely to be contained in the form of point defects, which increase with chemical impurities (*12*, *17*).

We measured the abundance of hydrogen in Mg-perovskite, magnesiowüstite, and Ca-perovskite synthesized in the natural peridotitic composition. The mineral phases were synthesized at high pressure and high temperature in a multianvil apparatus. Three starting materials were prepared as mixtures of Mg-free KLB-1 peridotite gel and brucite. $CaSiO_3$ glass or MgO and FeO reagents were also added to increase the volume of Ca-perovskite or magnesiowüstite (Table 1). The fine powders of the starting materials were loaded into $Au_{75}Pd_{25}$ capsules and then sealed. We used an 8/3 assembly (8-mm octahedron edge length and 3-mm truncated edge length of tungsten carbide). The experimental temperature was monitored with the use of a W_5Re-$W_{26}Re$ thermocouple that was inserted axially into the octahedral assembly. Three experiments were performed at a pressure of 25.5 GPa and at 1600° to 1650°C. The details of the experimental configuration and the pressure calibration are described elsewhere (*18*). Run durations were 60 to 75 min. The samples were quenched at a rate of 1000°C/s, and the recovered samples were examined with an electron probe microanalyzer. The major element compositions of the three synthesized minerals are shown in Table 1. In all the experiments, they coexisted with melts, and their size was larger than 40 μm in general. Ca-perovskite was pressure-unquenchable and converted to the amorphous state at ambient pressure.

In the secondary ion mass spectrometry (SIMS) analysis (*19*–*21*), each sample was mounted together with two standards (a natural hornblende containing 1.66 wt% H_2O and a H_2O-free $MgSiO_3$ perovskite). They were measured under the same conditions to have constant background signals correlated with the hydrogen ions. Surface-correlated water in the sample, such as water adsorbed on the surface and in micro-cracks introduced by polishing, was removed by sputtering the surface of the sample and monitoring the profile of the hydrogen intensity with sputter time (*20*, *22*). All analytical points showed the steady state of hydrogen intensity. The spot size of the primary ion beam (~10 μm) was smaller than the size of the grains analyzed in these measurements. Accordingly, we were able to avoid grain boundary effect. The analyzed water contents are shown in Table 2. The dispersion of each analytical point in the same phase may be due to the change in hydrogen background signals and the sample heterogeneity. The results show that Mg-perovskite and magnesiowüstite each contain ~0.2 wt% and that Ca-perovskite con-

Table 1. Experimental conditions and representative microprobe analyses of the run products. MgPv, Mg-perovskite; CaPv, Ca-perovskite; Mw, magnesiowüstite; St, stishovite.

	C157		C165		C183	
Run conditions						
Pressure (GPa)	25.5		25.5		25.5	
Temp. (°C)	1600		1620		1650	
Time (min)	75		60		60	
Products	MgPv+CaPv+St+melt		MgPv+CaPv+St+melt		MgPv+Mw+melt	
Molar compositions						
(O = 24)	MgPV	CaPv	MgPv	CaPv	MgPv	Mw
Si	7.324	7.786	7.173	7.911	7.353	0.118
Ti	0.003	0.013	0.012	0.033	0.009	—
Al	0.801	0.056	0.946	0.084	0.564	0.073
Cr	0.027	—	0.027	0.002	0.023	0.018
Fe	0.883	0.012	0.905	0.025	1.013	1.818
Mg	7.097	0.028	7.145	0.046	7.261	21.687
Ca	9.019	8.078	0.031	7.708	0.009	—
Na	—	0.015	0.005	0.015	0.005	0.030
K	0.002	0.008	—	—	—	—
H	0.209	0.380	0.173	0.392	0.220	0.217
Total	16.364	16.375	16.417	16.217	16.457	23.960

Starting materials

C157: 75.5 wt% KLB-1 gel + 11.0 wt% $CaSiO_3$ + 13.5 wt% H_2O

C165: 64.0 wt% KLB-1 gel + 25.0 wt% $CaSiO_3$ + 11.0 wt% H_2O

C183: 42.5 wt% KLB-1 gel + 38.9 wt% MgO + 11.1 wt% FeO + 7.5 wt% H_2O

[1]Department of Earth and Planetary Sciences, Tokyo Institute of Technology, Meguro, Tokyo 152-8551, Japan. [2]Interactive Research Center of Science, Tokyo Institute of Technology, Meguro, Tokyo 152-8551, Japan.

*To whom correspondence should be addressed. E-mail: mmurakam@geo.titech.ac.jp

tains ~0.4 wt% H_2O. There were no systematic differences in H_2O contents between the samples, and this may suggest that the solubility of H_2O in each phase does not depend on the H_2O content in the coexisting melt (or fluid).

Infrared (IR) microspectroscopic measurements were also made on single crystals of both Mg-perovskite and magnesiowüstite in the run products #C165 and #C183 (*23*, *24*). The IR spectra were obtained from doubly polished large crystals (~100 μm in size). All the grains analyzed were checked to be single grains by cross-polarized microscope. To avoid the grain boundary effect, we handpicked the crystals from the sample capsule. We found OH stretching bands at ~3690, ~3600, ~3410, and ~3340 cm^{-1} in the Mg-perovskite and at ~3620, ~3520, and ~3400 cm^{-1} in the magnesiowüstite (Fig. 1, A and B). The highest peak positions around 3400 cm^{-1} of Mg-perovskite and magnesiowüstite are similar to previous spectral measurements for the $MgSiO_3$-perovskite (*15*, *16*). We confirmed that the absorption intensity of the same single crystal of Mg-perovskite analyzed at same direction was proportionally reduced with thickness of a crystal from 50 to 20 μm. This result indicates that the adsorbed water on the sample surface is negligible in our measurements. The variation of band intensity in different grains (Fig. 1, A and B), therefore, might be due to heterogeneity of water contents in these minerals. The polarization anisotropy of IR spectra are presented in Fig. 1, C and D. Both the polarized spectra of Mg-perovskite and magnesiowüstite changed with changing sample orientation from 0° to 90°. This indicates that the water species observed in Mg-perovskite and magnesiowüstite are crystallographically oriented structural waters. Moreover, neither sub-μm inclusions nor sub-grain boundaries were observed in the single crystal of Mg-perovskite by the transmission electron microscopy (TEM; JEOL-2010). This observation shows that the hydroxyls should be in the crystal structure of Mg-perovskite. The relatively broad absorption spectra in the present IR analyses may indicate more complex speciation of water (*25*) than that formed in the simple $MgSiO_3$ system. We estimated the water content in the Mg-perovskite and magnesiowüstite with the use of unpolarized IR absorption data and on the basis of the Beer-Lambert law (*26*). The results show that Mg-perovskite contains ~0.1 wt% H_2O, and magnesiowüstite contains ~0.2 wt% H_2O. This seems consistent with that of SIMS analyses.

The oxygen defect substitution correlated with the trivalent ions such as Al^{3+} and Fe^{3+} has been proposed for the incorporation of H_2O in Mg-perovskite (*12*). Our study shows that Mg-perovskite including some Al_2O_3 and Fe_2O_3 can contain ~2000 parts per million (ppm) H_2O, whereas pure $MgSiO_3$-perovskite contains much less water (<60 ppm H_2O) (*15*, *16*). If it is assumed that such oxygen defect substitutions only by Al^{3+} are the dominant mechanism of H_2O solubility in this phase, then it is shown that 19 to 39% of Al^{3+} is incorporated with these substitutions based on the water contents studied here. This study also shows that magnesiowüstite can contain large amounts

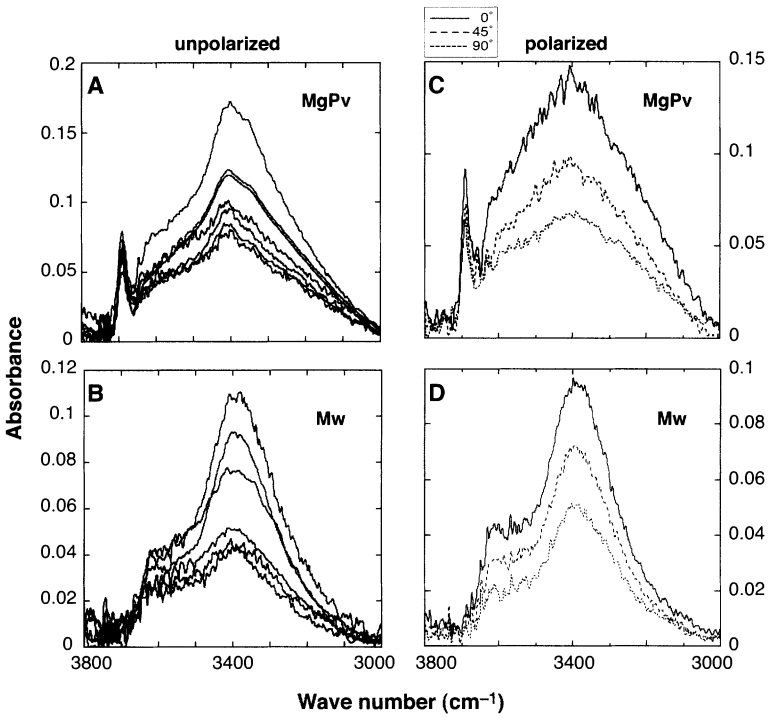

Fig. 1. Unpolarized infrared spectra with a 20 μm by 20 μm aperture of Mg-perovskite and magnesiowüstite single grains obtained from run product #C183. Thickness of the samples are ~20 μm for magnesiowüstite and ~80 μm for Mg-perovskite (**A** and **B**). Polarized infrared spectra with a 20 μm by 20 μm aperture of Mg-perovskite (run #C165) and magnesiowüstite (run #C183) and a sample thickness of ~50 and ~20 μm, respectively (**C** and **D**). Polarized spectra are obtained by rotating the sample on the rotary sample stage under IR microscope with a polarized IR beam.

Table 2. H_2O contents of each analytical point measured by SIMS. Standard deviation was determined by count statistics of secondary ion intensities at steady state H^+ emission.

Mineral phase	Run no.	H_2O content (wt%)	Error (2σ)	Average (wt%)
Mg-perovskite	C157	0.25	0.02	
		0.36	0.01	
		0.16	0.01	
		0.11	0.00	
		0.28	0.01	0.23
	C165	0.35	0.01	
		0.15	0.01	
		0.25	0.01	
		0.12	0.01	
		0.16	0.02	
		0.28	0.01	0.19
	C183	0.34	0.01	
		0.14	0.01	0.24
Ca-perovskite	C157	0.34	0.04	
		0.44	0.04	
		0.32	0.03	0.37
	C165	0.51	0.03	
		0.37	0.02	
		0.22	0.01	
		0.49	0.06	
		0.31	0.02	0.38
Magnesiowüstite	C183	0.21	0.01	
		0.10	0.01	
		0.25	0.02	
		0.18	0.02	0.19

of water, whereas the pure MgO-periclase coexisting with $MgSiO_3$-perovskite and melt can contain only ~2 ppm H_2O (*16*). Magnesiowüstite is likely to include some Fe^{3+} (*27*). The coupled substitution $2M^{2+} = Fe^{3+} + H^+$ may be necessary to incorporate hydrogen in this phase. Ca-perovskite is a major carrier of trace elements in the lower mantle (*28*). Our study shows that Ca-perovskite has a higher solubility of H_2O than the other two phases. However, the analyses were made after Ca-perovskite became amorphous at ambient pressure, so further investigation on its H_2O solubility with a perovskite structure is needed.

Our results suggest that the lower mantle can potentially store considerable amounts of water. A lower mantle, consisting of 79 wt% Mg-perovskite, 16 wt% magnesiowüstite, and 5 wt% Ca-perovskite (*11*), can contain 0.2 wt% H_2O. When this capacity is integrated over the mass of the lower mantle, the total mass of water is ~5 times that of oceans. This amount is comparable to that in the transition zone (~6 times more than the oceans), where 3.3 and 2.2 wt% H_2O can be included in wadsleyite and ringwoodite, respectively (*5*, *7*). The considerable amount of hydrogen can be stored in deep reservoirs such as the transition zone, lower mantle, and core (*5*–*8*).

The high solubility of H_2O in representative lower mantle minerals also has implications for the rheological properties of the lower mantle (*29*). The presence of water in a crystal structure can reduce the strength of a mineral and control creep mechanisms (*2*, *6*). The water may be transported into the lower mantle by the subduction of hydrated slabs, and may be released upon decomposition of DHMS phases such as phase D, which contains ~10 wt% H_2O, around 1200 km depth (*9*). Hydrogen may be also added to the lower mantle from the hydrogen-saturated outer core as H_2O (*8*). Lower mantle minerals would absorb this released H_2O and would be considerably softened due to the relaxation around the defects. Accordingly, flow of material would be expected along the down-going slabs and along the bottom of the mantle.

References and Notes

1. A. E. Ringwood, *Geochem. J.* **11**, 111 (1977).
2. S. Karato, M. S. Paterson, J. D. FitzGerald, *J. Geophys. Res.* **91**, 8151 (1986).
3. H. Iwamori, *Earth Planet. Sci. Lett.* **160**, 65 (1998).
4. T. Kawamoto, R. L. Herving, J. R. Holloway, *Earth Planet. Sci. Lett.* **142**, 58 (1996).
5. T. Inoue, H. Yurimoto, Y. Kudoh, *Geophys. Res. Lett.* **22**, 117 (1995).
6. D. L. Kohlstedt, H. Keppler, D. C. Rubie, *Contrib. Mineral. Petrol.* **123**, 345 (1996).
7. T. Inoue, D. J. Weidner, P. A. Northrup, J. B. Parise, *Earth Planet. Sci. Lett.* **160**, 107 (1998).
8. T. Okuchi, *Science* **278**, 1781 (1997).
9. S. R. Shieh, H. K. Mao, R. J. Hemley, L. C. Ming, *Earth Planet. Sci. Lett.* **159**, 13 (1998).
10. S. E. Kesson, J. D. Fitz Gerald, J. M. Shelley, *Nature* **393**, 252 (1998).
11. B. J. Wood, *Earth Planet. Sci. Lett.* **174**, 341 (2000).
12. A. Navrotsky, *Science* **284**, 1788 (1999).
13. C. McCammon, *Nature* **387**, 694 (1997).
14. J. P. Brodholt, *Nature* **407**, 620, (2000).
15. C. Meade, J. A. Reffner, E. Ito, *Science* **264**, 1558, (1994).
16. N. Bolfan-Casanova, H. Kepler, D. C. Rubie, *Earth Planet. Sci. Lett.* **182**, 209 (2000).
17. D. R. Bell, G. R. Rossman, *Science* **255**, 1391 (1992).
18. K. Hirose, Y. Fei, S. Ono, T. Yagi, K. Funakoshi, *Earth Planet. Sci. Lett.* **184**, 567 (2001).
19. On SIMS analysis (Cameca ims-3F), a primary ion beam consisted of mass-filtered $^{16}O^-$, accelerated −12.5 kV, with a beam current of about 5 nA and a spot size of 10 to ~15 μm in diameter. Secondary ions were accelerated at 4.5 kV. The intensity of the positive secondary $^1H^+$, $^{30}Si^+$, $^{26}Mg^+$, and $^{44}Ca^+$ ions were measured under steady state secondary ion emissions. To reduce the background signals, the vacuuming level of the sample chamber was maintained at 0.2 μPa, and a cold trap by liquid nitrogen was employed. The samples were coated with Au film of ~20 nm thickness to eliminate electrostatic charging. Two standard materials were measured repeatedly in every analysis of the sample. Accordingly, the calibration lines were constructed with each analysis. Other analytical and instrumental conditions were similar to previous works (*20*, *21*).
20. H. Yurimoto, M. Kurosawa, S. Sueno, *Geochim. Cosmochim. Acta* **53**, 751 (1989).
21. I. Miyagi, H. Yurimoto, *Bull. Volcanol. Soc. Jpn.* **40**, 349 (1995).
22. The counting time of SIMS analysis by one cycle was 2 seconds for $^{30}Si^+$, $^{26}Mg^+$, and $^{44}Ca^+$ ions, and was 10 s for $^1H^+$ ion. All the samples were measured by 250 cycles. Before measurement, pre-sputtering was set at about 100 cycles to obtain a steady state of hydrogen intensity.
23. In the IR study, the IR light emitted by a light source through a Ge-coated KBr beam splitter is focused on a sample by means of Cassegrain mirrors with a magnification of 16. This light passes through a sample, to a MCT (HgCdTe) detector. Several hundreds to thousands scans were accumulated with 4 cm^{-1} resolution to obtain IR absorption spectra of the sample.
24. S. Nakashima *et al.*, *Tectonophysics* **245**, 263 (1995).
25. R. D. Aines, G. R. Rossman, *J. Geophys. Res.* **89**, 4059 (1984).
26. Beer-Lambert law can be expressed as $A_i = ct\varepsilon_i$, where A_i is integrated absorbance, c is molar concentrations of hydrogen, t is the thickness of the sample, and ε_i is the integrated molar absorption coefficient calculated from the method described in (*30*). The error in this estimation is predominantly influenced by ε_i, t, and the anisotropy of the mineral. We adopted the orientation factor ($\zeta = 1/3$).
27. D. J. Frost, F. Langenhorst, P. A. van Aken, *Phys. Chem. Minerals* **28**, 455 (2001).
28. W. Wang, T. Gasparik, R. P. Rapp, *Earth Planet. Sci. Lett.* **181**, 291 (2000).
29. Q. Williams, R. J. Hemley, *Annu. Rev. Earth Planet. Sci.* **29**, 365 (2001).
30. E. Libowitzky and G. R. Rossman, *Am. Mineral.* **82**, 1111 (1997).

31. We thank E. Takahashi, S. Maruyama, and B. F. Windley for discussions and comments, and T. Kawamoto for providing gel starting material. We are grateful to I. Katayama for help with the infrared measurements. TEM analyses were performed at the University of Tokyo.

5 September 2001; accepted 5 February 2002

Repeated and Sudden Reversals of the Dipole Field Generated by a Spherical Dynamo Action

Jinghong Li,[1]* Tetsuya Sato,[1,2]† Akira Kageyama[1,2]

Using long-duration, three-dimensional magnetohydrodynamic simulation, we found that the magnetic dipole field generated by a dynamo action in a rotating spherical shell repeatedly reverses its polarity at irregular intervals (that is, punctuated reversal). Although the total convection energy and magnetic energy alternate between a high-energy state and a low-energy state, the dipole polarity can reverse only at high-energy states where the north-south symmetry of the convection pattern is broken and the columnar vortex structure becomes vulnerable. Another attractive finding is that the quadrupole mode grows, exceeding the dipole mode before the reversal; this may help to explain how Earth's magnetic field reverses.

Earth's magnetic field is believed to be generated by dynamo action in a rotating electrically conducting fluid (*1*–*3*). The magnetic field of Earth is dipole-dominated and suddenly reverses its polarity at irregular intervals (*4*, *5*).

Three-dimensional magnetohydrodynamic simulations in recent years have succeeded in demonstrating the self-excitation of the dipole field (*6*–*8*). In the Glatzmaier-Roberts simulation (*6*), reversal of the generated dipole field was also observed. On the other hand, the Kageyama-Sato model obtained a flip-flop transition of the total magnetic and convection energies, which was associated with the reversal of the dipole field (*9*). Glatzmaier *et al.* (*10*) studied the effects of nonuniformity of heat flux pattern on the reversal to find the role of the nonuniform heat flux. Coe *et al.* (*11*) described the evolution of the morphology and/or spectral energy of simulated magnetic fields during reversals. Although the previous reversal studies have succeeded in demonstrating the occurrence

[1]Department of Fusion Science, The Graduate University for Advanced Studies, Toki, 509-5292, Japan. [2]Theory and Computer Simulation Center, National Institute for Fusion Science, Toki, 509-5292, Japan.

*Permanent address: Institute of Applied Physics and Computational Mathematics, Post Office Box 8009, Beijing 100088, China.

†To whom correspondence should be addressed. E-mail: sato@tcsc.nifs.ac.jp